

## Spectral Analysis of Square-wave Pulse Density Modulation: An Analytical Approach

Jakson Paulo Bonaldo\* and José Antenor Pomilio\*

\*School of Electrical and Computer Engineering, Campinas, Brazil

### ABSTRACT

The pulse density modulation technique has been used in resonant power converters because its ability to maintains soft-switching for any level of output power. The sub harmonics of the switching frequency are in general undesired and are seen as a drawback. In this work are developed analytical equations to express the harmonics and sub harmonics components of a PDM signal. It is still analyzed the PDM parameters variation and their effects in the frequency spectra.

**Keywords** - Double Fourier Series, Pulse Density Modulation, Ozone Generation, Resonant Converters

### I. INTRODUCTION

In many applications in which it is sufficient to control the average power in a relatively long time interval it is possible to modulate the output power by using the PDM - Pulse Density Modulation. This modulation technique allows operation with constant switching frequency and pulse width, controlling the power by varying the pulses in a given time base, while keeping soft switching capability in the whole power range for which the converter was designed [1]. It is still possible to simultaneously control the PDM modulation ratio and the duty cycle allowing a finer and more accurate adjust of the output power delivered to a given load [2].

The PDM control may be applied on an extended range of high frequency high power resonant converters. The main applications where square wave PDM control are commonly applied to are power converters intended to be used for ozone generation [3][4][5], high power welding machines, high frequency induction heating for plasma applications [6] and power supplies with inherent soft switching capability.

As an example of application of PDM modulation one can take the a typical ozone generation converter, as shown in Fig. 1 where the load has a capacitive behavior allowing resonant operation since the transformer has significant inductance., as shown in Fig. 2 [7]. The transformer can became saturated if the inverter produces a non zero average voltage. Such unbalance can be originated with small differences in the power

switches or gate drives. The DC blocking capacitor adds an additional low frequency series resonance, as shown in Fig. 3. Such resonance can be excited by low-frequency components present in the PDM signal, as illustrated in Figure 6. If the magnetizing inductance saturates the frequency in which the series resonance occurs can change, leading the circuit (transformer plus ozone cell) to an unknown and variable operation point which should be avoided for safe operation of the circuit [8].

Fig.4 shows a typical PDM pulse train and the resulting current when these pulses are applied to the ozone generating cell. In such application it is useful to investigate whether there are or not harmonic and sub harmonic components in the low frequency range which could lead to a malfunctioning of the power converter.

In [9] it is shown a methodology to estimate the PDM spectra observing the modulated current. However, in this work is proposed a new approach to accurately calculate the PDM spectra based only on the voltage of the PDM pulse train by means of analytical equations based on the PDM signal. These equations can give to the designer a fast way to check whether the system against resonances which may be excited by the sub harmonics of the PDM signal. It is also possible to determine for what range of PDM densities or pulse widths the system operation is sage.

It is important state that the application of the proposed analysis is not limited to ozone generation devices, but it can be fully applicable to any other application related to the use of PDM modulation in electronics power converters.

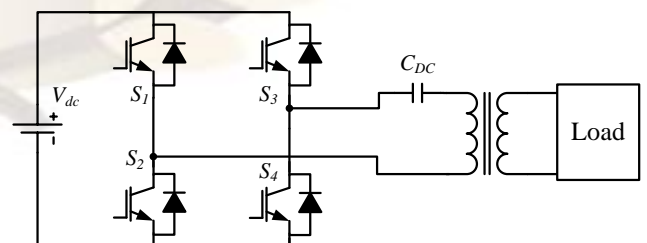


Fig. 1 - Typical resonant converter used for ozone generation.

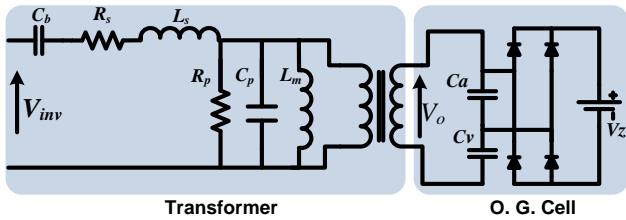


Fig. 2 – Transformer and load model, including DC blocking capacitor.

This work is organized in more three sections. In the second section it is explained the general theory behind the PDM spectral analysis. Section three deals with the unipolar PDM pulses which could be applicable on DC-DC power converters when they are operating with PDM modulation. Finally, section four brings the analysis of the bipolar PDM pulses which are the main issue of this work.

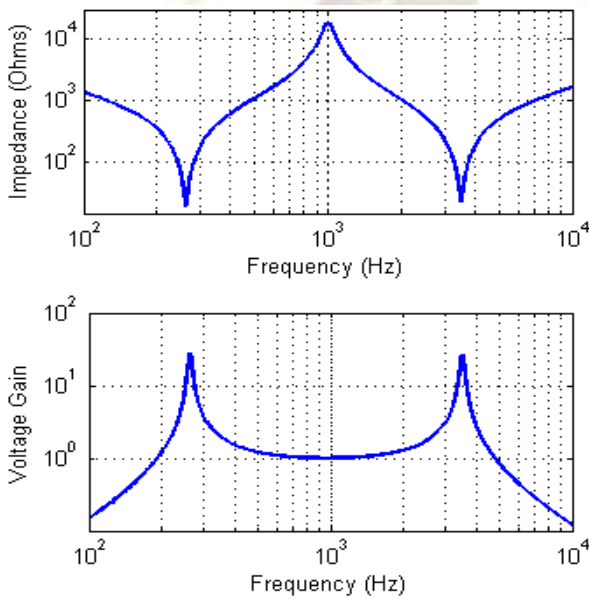


Fig. 3 – Input impedance and voltage gain.

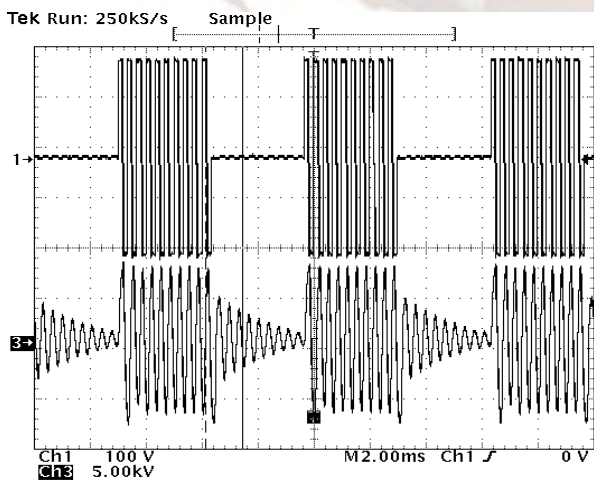


Fig. 4 - PDM pulses applied on an ozone generating cell.

## II. PDM – BASIS OF PULSE DENSITY MODULATION SPECTRAL ANALYSIS

Holmes and Lipo [10] show a methodology for determining the spectrum of a Sinusoidal Pulse Width Modulation – SPWM. Based on the concept of sinusoidal switching cell, this paper considers a switching cell for a rectangular wave, whereby it becomes possible to obtain the analytical expression of the frequency spectrum for rectangular pulse density modulation.

The concept of switching cell can be used to find the Double Fourier Series (DFS) of a signal given by  $f(t)$ , which is composed of a carrier and a modulating waveform. The modulating is also known as the reference signal. The unit switching cell identifies edges within for which the function  $f(t)$  is constant for periodic variation of the carrier  $x(t)$  and modulating  $y(t)$  signals.

The function  $f(t) = f[x(t), y(t)]$ , within each region boundary of the unit cell, represents the resulting voltage in the arms of a single-phase H-bridge inverter. For a low frequency reference, or modulating, rectangular-type unit cell is proposed as shown in Figure 1.

It can happen variations in both, the pulse width of the low frequency reference signal and in the high frequency carrier wave, that is the converter switching frequency. Therefore, the cell inner contour is determined by  $\Delta$  and  $\delta$ , where:

- $\Delta \rightarrow$  duty-cycle of the reference low frequency
- $\delta \rightarrow$  duty-cycle of the high frequency carrier

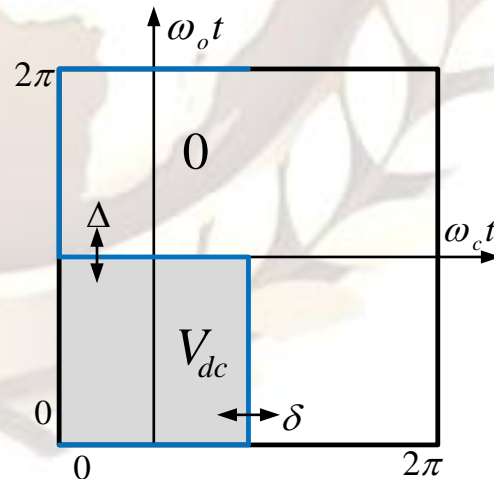


Fig. 1 – Rectangular Switching Cell.

The range of  $\Delta$  and  $\delta$  are between 0 and  $2\pi$ . The variation of  $\Delta$  modify the PDM pulse density, what means change the duty cycle of the modulating signal increasing the high frequency pulses inside a low frequency period, leading to changes in the average power delivered to a given

load. Variations in  $\delta$  change the width of the high frequency pulses, affecting the voltage value.

Fig. 6.a shows a grid consisting of the unit cell replication and Fig. 6.b shows the resulting modulated signal. While the line with slope  $\omega_o / \omega_c$  is over the gray area of the unit cell, the resulting voltage value is equal to  $V_{DC}$ . The voltage returns to zero when the line crosses the boundary and reaches the white region of the unit cell, thus generating the pulse density modulated signal.

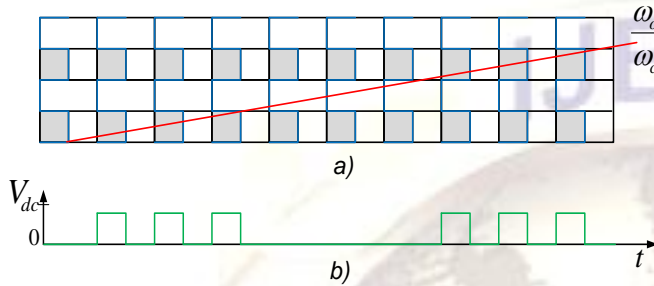


Fig. 6 – Arrangement of unit cells which originates the PDM signal.

The general form of the Double Fourier Series is given in (1), in which the first term refers to the average value. The second term refers to the harmonics of the base band. The third term consists of harmonics of the carrier and the fourth consists of the sideband harmonic of the carrier.

$$f(x, y) = \frac{A_{00}}{2} + \sum_{n=0}^{\infty} [A_{0n} \cos(ny) + B_{0n} \sin(ny)] + \sum_{m=1}^{\infty} [A_{m0} \cos(mx) + B_{m0} \sin(mx)] + \sum_{m=0}^{\infty} \sum_{n=-\infty}^{\infty} [A_{mn} \cos(mx + ny) + B_{mn} \sin(mx + ny)] \quad (1)$$

Or, in the general form:

$$f(x, y) = \sum_{m=0}^{\infty} \sum_{n=-\infty}^{\infty} [A_{mn} \cos(mx + ny) + B_{mn} \sin(mx + ny)] \quad (2)$$

Where:

$$x(t) = \omega_c t + \theta_c \quad y(t) = \omega_o t + \theta_o$$

$\omega_c \rightarrow$  carrier angular frequency

$\theta_c \rightarrow$  carrier phase angle

$\omega_o \rightarrow$  reference angular frequency

$\theta_o \rightarrow$  reference phase angle

The indices  $m$  and  $n$  define the harmonic frequencies of the carrier and the modulating wave, respectively. A combination of these indices turn in

side band harmonics. For  $m=n=0$  it is defined the first term of the DFS, which corresponds to the average value of the pulse width modulated signal. For  $m=0$ , the harmonic frequencies are defined by  $n$ , being named as base band harmonics. For  $n=0$  the harmonic frequencies are due to the carrier and defined by  $m$ , named carrier harmonics. The sidebands harmonics are created when  $m \neq 0$  and  $n \neq 0$ .

The DFS coefficients, in the trigonometric form, can be calculated as follows, where the limits of integration must be used according to the switching cell.

$$A_{mn} = \frac{1}{2\pi^2} \int_0^{2\pi} \int_0^{2\pi} f(x, y) \cos(mx + ny) dx dy \quad (3)$$

$$B_{mn} = \frac{1}{2\pi^2} \int_0^{2\pi} \int_0^{2\pi} f(x, y) \sin(mx + ny) dx dy \quad (4)$$

Or, in the complex form:

$$C_{mn} = A_{mn} + jB_{mn} = \frac{1}{2\pi^2} \int_0^{\Delta} \int_0^{\delta} f(x, y) e^{j(mx+ny)} dx dy \quad (5)$$

The DFS analysis is initially developed for an unipolar PDM waveform, as shown in Fig. 7, which is expressed in terms of the DFS coefficients. The unipolar DFS is then expanded to the bipolar DFS by means of the sum of two unipolar waveforms shifted in time by the angle corresponding to the complementary carrier duty-cycle.

### III. DFS CALCULATION OF AN UNIPOLAR PDM WAVEFORM

The switching cell showed on Fig. 5 is used to perform the DFS calculation of an Unipolar PDM waveform defining a function  $f(x, y)$  which does not need to be integrated all over the periods, but just until the  $\Delta$  and  $\delta$  limits. The DFS calculation is carried on apart for each kind of coefficient as depicted bellow.

*Average Coefficient*

$$C_{00} = A_{00} + jB_{00} = \frac{1}{2\pi^2} \int_0^{\Delta} \int_0^{\delta} V_{dc} e^{j(0 \cdot x + 0 \cdot y)} dx dy = \frac{V_{dc}}{2\pi^2} \int_0^{\Delta} \int_0^{\delta} dx dy = \frac{V_{dc}}{2\pi^2} \int_0^{\Delta} \delta dy = \frac{V_{dc}}{2\pi^2} \Delta \delta \quad (6)$$

*Baseband Coefficients*

$$C_{0n} = A_{0n} + jB_{0n} = \frac{1}{2\pi^2} \int_0^{\Delta} \int_0^{\delta} V_{dc} e^{j(0 \cdot x + ny)} dx dy =$$

$$= \frac{V_{dc}}{2n\pi^2} \delta [j + \sin(n \cdot \Delta) - j \cos(n \cdot \Delta)] \quad (7)$$

Carrier Coefficients

$$C_{m0} = A_{m0} + jB_{m0} = \frac{1}{2\pi^2} \int_0^{\Delta} \int_0^{\delta} V_{dc} e^{j(m \cdot x + 0 \cdot y)} dx dy =$$

$$= \frac{V_{dc}}{2m\pi^2} [j + \sin(m \cdot \delta) - j \cos(m \cdot \delta)] \cdot \Delta \quad (8)$$

Carrier Sideband Coefficients

$$C_{mn} = A_{mn} + jB_{mn} = \frac{1}{2\pi^2} \int_0^{\Delta} \int_0^{\delta} V_{dc} e^{j(mx + ny)} dx dy = \quad (9)$$

$$= \frac{V_{dc}}{2mn\pi^2} \left\{ \begin{aligned} &\cos(\Delta n) + \cos(\delta m) - \cos(\Delta n + \delta m) - 1 + \\ &+ j[\sin(\Delta n) + \sin(\delta m) - \sin(\Delta n + \delta m)] \end{aligned} \right\}$$

The function  $f(x, y, t)$ , which denote the Unipolar

$$f(x, y, t) = \frac{V_{dc}}{4\pi} \Delta \delta + \sum_{n=0}^{\infty} \left[ \frac{V_{dc}}{2n\pi^2} \delta \sin(n \cdot \Delta) \cdot \cos(n\omega_o t + n\theta_0) + \frac{V_{dc}}{2n\pi^2} \delta [1 - \cos(n \cdot \Delta)] \cdot \sin(n\omega_o t + n\theta_0) \right] +$$

$$+ \sum_{m=1}^{\infty} \left[ \frac{V_{dc}}{2m\pi^2} \Delta \cdot \sin(m \cdot \delta) \cdot \cos(m\omega_c t + m\theta_c) + \frac{V_{dc}}{2m\pi^2} \Delta [1 - \cos(m \cdot \delta)] \cdot \sin(m\omega_c t + m\theta_c) \right] +$$

$$+ \sum_{m=0}^{\infty} \sum_{n=-\infty}^{\infty} \left[ \frac{V_{dc}}{2mn\pi^2} [\cos(\Delta n) + \cos(\delta m) - \cos(\Delta n + \delta m) - 1] \cdot \cos(m\omega_c t + m\theta_c + n\omega_o t + n\theta_0) + \right.$$

$$\left. + \frac{V_{dc}}{2mn\pi^2} [\sin(\Delta n) + \sin(\delta m) - \sin(\Delta n + \delta m)] \cdot \sin(m\omega_c t + m\theta_c + n\omega_o t + n\theta_0) \right] \quad (10)$$

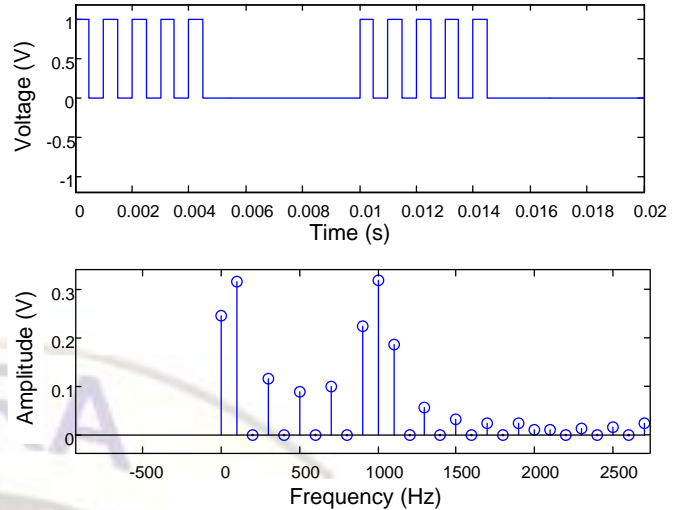


Fig. 7 – DC biased PDM signal (bottom) and its spectrum (top).

PDM signal in the time domain, can be synthesized or reconstructed from the coefficients calculated above by means of (10).

Fig. 7 shows an example of Unipolar PDM signal which has unitary voltage amplitude. The modulating pulse density is 0.5 corresponding to  $\Delta = 2\pi \cdot 0.5$  and the carrier pulse density is 0.5 corresponding to  $\delta = 2\pi \cdot 0.5$ . Fig. 3 also shows the spectrum of this PDM obtained by the FFT of the PDM signal. Fig. 8 compares the spectrum obtained via FFT and the spectrum analytically calculated using the equations develop early in this section.

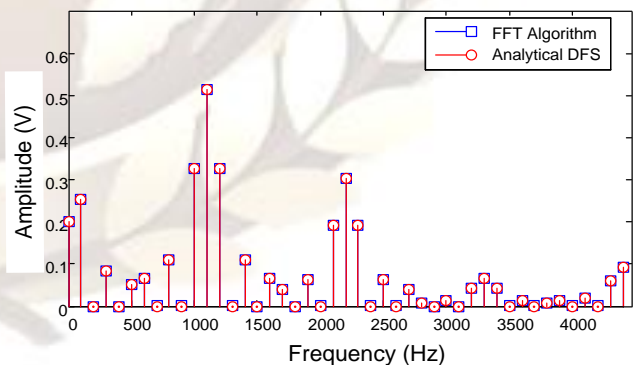


Fig. 8 – Comparison of spectra of the waveform shown in Fig. 3 with the spectra analytically calculated.

Fig. 8 clearly shows that the FFT spectrum of the Unipolar PDM signal matches exactly the spectrum obtained when applying the mathematical expressions developed. This result validate the

expressions previously developed for the Unipolar PDM signal.

The next section deal with the calculation of the DFS coefficients for the Bipolar PDM signal which is an extension of the analysis presented in the current section.

#### IV. DFS CALCULATION OF A BIPOLAR PDM WAVEFORM

The waveform of the bipolar PDM signal can be obtained by the difference between  $f(x, y)|_{\theta_c=0}$  and  $f(x, y)|_{\theta_c=\gamma}$ , where:  $\gamma = 2\pi - \delta$  is complementary part of the width of high frequency pulses.

Therefore,

$$f_{PDM}(x, y) = f(x, y)|_{\theta_c=0} - f(x, y)|_{\theta_c=\gamma} \quad (11)$$

The physical meaning of (11) is better understood when analyzing how the PDM waveform is generated in an single-phase full-bridge converter. The first arm of the inverter generates the PDM pulses given by  $f(x, y)|_{\theta_c=0}$  and the second arm generates the pulses given by  $f(x, y)|_{\theta_c=\gamma}$ . So, the combination of both signal make up the Bipolar PDM signal which is in fact applied over any connected load.

The signal generated by the inverter is given by (12) which express the Bipolar PDM signal in time domain. For the sake of simplicity the final shape of

the coefficients is not shown, since they can be promptly extracted from (12).

In order to validating the decomposition of the Bipolar PDM signal the following figures shown the frequency and time domain plots when varying the modulating index of the reference signal  $\Delta$  and the carrier modulating index  $\delta$  which also dictates the pulse width of the carrier waveform.

As shown in Fig. 9, Fig. 10 and Fig. 11, the amplitude of the carrier varies proportionally to the duty cycle of the modulating wave in proportion to  $\Delta$ . Variations in the pulse width of the carrier,  $\delta$ , does not exert a major influence on the amplitude of the carrier. However, are of great importance for the sidebands to the carrier, and especially for the harmonics in the baseband and the average level. This feature can be used to make the control of the voltage average level.

Beside it is possible and in many times desired to control both the pulse density of the modulating signal and the pulse width of the carrier signal. This results shown that using carrier duty cycles different from 0.5 which is equivalent to  $\delta \neq \pi$  generates low frequency harmonics and, as stated before, this kind of harmonics are drawbacks for some applications, mainly when using a DC block capacitor.

$$f_{PDM}(x, y) = \frac{V_{dc}}{4\pi} \Delta (\delta - \gamma) + \sum_{n=0}^{\infty} \left\{ \frac{V_{dc}}{2n\pi^2} [(\delta - \gamma) \sin(n \cdot \Delta) \cdot \cos(n\omega_o t + n\theta_o) + (\delta - \gamma) [1 - \cos(n \cdot \Delta)] \cdot \sin(n\omega_o t + n\theta_o)] \right\} +$$

$$+ \sum_{m=1}^{\infty} \left\{ \frac{V_{dc}}{2m\pi^2} \Delta \left[ \{ \sin(m \cdot \delta) - (\Delta \cdot \sin(m \cdot \delta) \cos(m\gamma) - [1 - \cos(m \cdot \delta)] \sin(m\gamma)) \} \cdot \cos(m\omega_c t) + \right. \right. \\ \left. \left. + \{ [1 - \cos(m \cdot \delta)] - (\Delta [1 - \cos(m \cdot \delta)] \cos(m\gamma) - \sin(m \cdot \delta) \sin(m\gamma)) \} \cdot \sin(m\omega_c t) \right] \right\} +$$

$$+ \sum_{m=0}^{\infty} \sum_{n=-\infty}^{\infty} \left\{ \frac{V_{dc}}{2mn\pi^2} \left[ \begin{array}{l} \left[ \begin{array}{l} [\cos(\Delta n) + \cos(\delta n) - \cos(\Delta n + \delta n) - 1] - \\ - [\cos(\Delta n) + \cos(\delta n) - \cos(\Delta n + \delta n) - 1] \cos(m\gamma) - \\ - [\sin(\Delta n) + \sin(\delta n) - \sin(\Delta n + \delta n)] \sin(m\gamma) \end{array} \right] \cdot \cos(m\omega_c t + n\omega_o t + n\theta_o) + \\ \left[ \begin{array}{l} [\sin(\Delta n) + \sin(\delta n) - \sin(\Delta n + \delta n)] - \\ - [\sin(\Delta n) + \sin(\delta n) - \sin(\Delta n + \delta n)] \cos(m\gamma) + \\ + [\cos(\Delta n) + \cos(\delta n) - \cos(\Delta n + \delta n) - 1] \sin(m\gamma) \end{array} \right] \cdot \sin(m\omega_c t + n\omega_o t + n\theta_o) \end{array} \right] \right\} \quad (12)$$

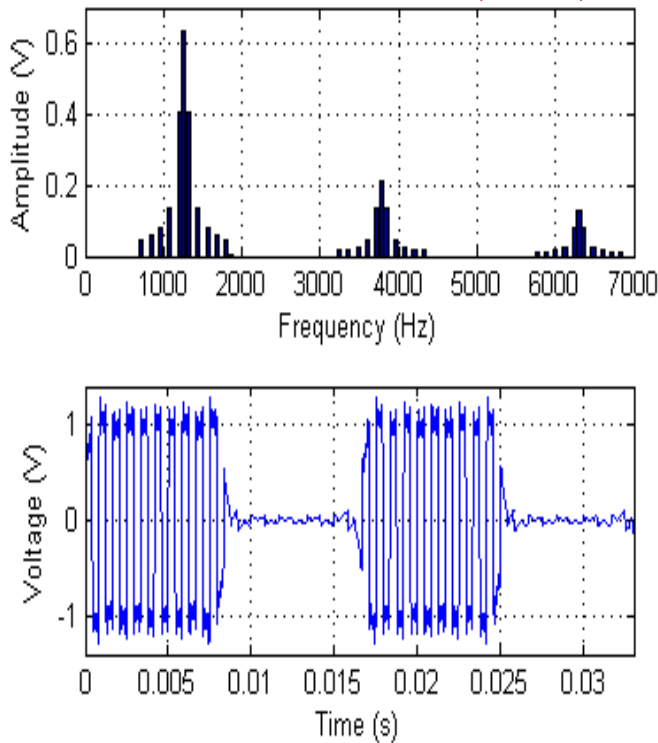


Fig. 9 – PDM spectrum and waveform for  $\Delta = \pi$  and  $\delta = \pi$ .

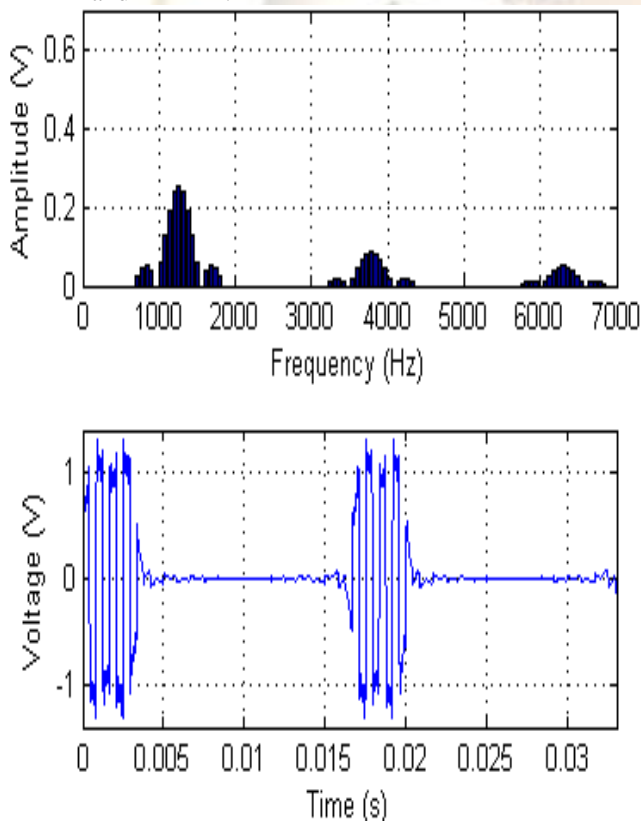


Fig. 10 – PDM spectrum and waveform for  $\Delta = 2\pi \cdot 0,2$  e  $\delta = \pi$

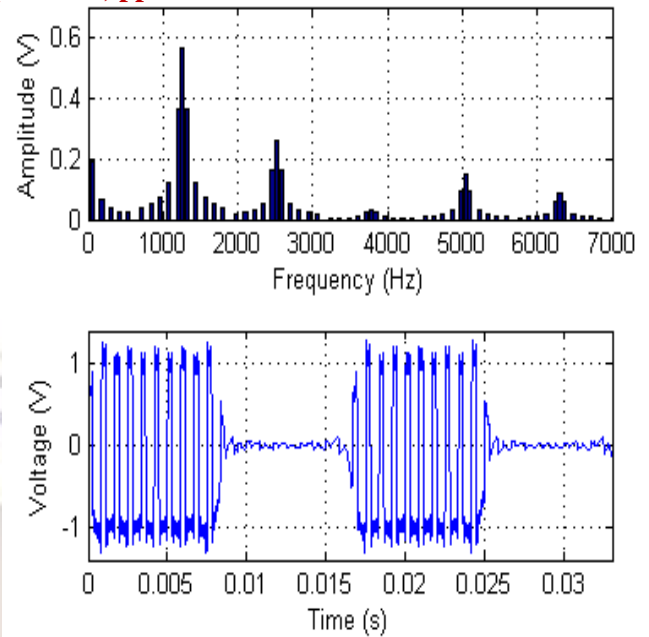


Fig. 11 – PDM spectrum and waveform for  $\Delta = \pi$  e  $\delta = 0,35 \cdot 2\pi$

## V. CONCLUSIONS

This work has presented a new approach to analytically determine the spectrum of a square wave PDM modulated signal. Each spectral component can be obtained and analyzed against variations in modulation parameters like carrier pulse width and reference modulating index. Therefore, this tool could be useful for analyzing a given spectral component of interest and check out its behavior when changes occur in the PDM parameters, making possible to rapidly determine the amplitude of that component, whether it exists in the considered PDM signal.

## REFERENCES

- [1] Ahmed, N.A.; , "High-Frequency Soft-Switching AC Conversion Circuit With Dual-Mode PWM/PDM Control Strategy for High-Power IH Applications," Industrial Electronics, IEEE Transactions on , vol.58, no.4, pp.1440-1448, April 2011.
- [2] Amjad, M.; Salam, Z.; Facta, M.; Mekhilef, S.; , "Analysis and Implementation of Transformerless LCL Resonant Power Supply for Ozone Generation," Power Electronics, IEEE Transactions on , vol.28, no.2, pp.650-660, Feb. 2013.
- [3] Vijayan, T.; Patil, Jagadish G.; , "A model of the generation and transport of ozone in high-tension nozzle driven corona inside a novel diode," Review of Scientific Instruments , vol.83, no.12, pp.123304-123304-11, Dec 2012

- [4] J. Alonso, J. Garcia, A. Calleja, J. Ribas, and J. Cardesin, "Analysis, design, and experimentation of a high-voltage power supply for ozone generation based on current-fed parallel-resonant push-pull inverter", IEEE Transactions on Industry Applications, vol. 41, no. 5, pp. 1364–1372, Sept.-Oct. 2005.
- [5] Nakata, Y.; Itoh, J.; , "An experimental verification and analysis of a single-phase to three-phase matrix converter using PDM control method for high-frequency applications," Power Electronics and Drive Systems (PEDS), 2011 IEEE Ninth International Conference on , vol., no., pp.1084-1089, 5-8 Dec. 2011.
- [6] Vijayan, T.; Patil, J.G.; , "Temporal Development of Ozone Generation in Electron-Induced Corona-Discharge Plasma," Plasma Science, IEEE Transactions on , vol.39, no.11, pp.3168-3172, Nov. 2011.
- [7] J. P. Bonaldo. J. A. Pomilio, "Control Strategies for High Frequency Voltage Source Converter for Ozone Generation", Proc. of the IEEE International Symposium on Industrial Electronics, ISIE 2010, Bari, Italy, July 4 to 7, 2010, pp; 754-760.
- [8] L. Bolduc, A. Gaudreau, A. Dutil, "Saturation time of transformers under dc excitation", Elsevier Electric Power Systems Research Vol. 56, 2000, pp. 95–102.
- [9] H. Calleja, J.Pacheco, Frequency Spectra of Pulse-Density Modulated Waveforms, México, 2000.
- [10] D. G. Holmes and T. A. Lipo, Pulse width modulation for power converters: Principles and practice, Wiley Inter-Science, 2003. 724 p.